

Actin based propulsion: Intriguing interplay between material properties and growth processes

Karin John,* Philippe Peyla, Mourad Ismail, and Chaouqi Misbah†
LSP UMR5588, Université J. Fourier, BP 87 - 38402 Grenoble Cedex, France

Denis Caillerie
L3S-R, BP 53 - 38041 Grenoble Cedex 9, France

Annie Raoult
Laboratoire MAP5 UMR 8145, Université Paris Descartes,
45 rue des Saints Pères, 75270 Paris Cedex 06, France

Jacques Prost
Physico-Chimie, Institut Curie UMR168, 26 rue d'Ulm, 75248 Paris Cedex 05, France

Eukaryotic cells and intracellular pathogens such as bacteria or viruses utilize the actin polymerization machinery to propel themselves forward. Thereby, the onset of motion and choice of direction may be the result of a spontaneous symmetry-breaking or might be triggered by external signals and preexisting asymmetries, e.g. through a previous septation in bacteria.

Although very complex, a key feature of cellular motility is the ability of actin to form dense polymeric networks, whose microstructure is tightly regulated by the cell. These polar actin networks produce the forces necessary for propulsion but may also be at the origin of a spontaneous symmetry-breaking.

Understanding the exact role of actin dynamics in cell motility requires multiscale approaches which capture at the same time the polymer network structure and dynamics on the scale of a few nanometers and the macroscopic distribution of elastic stresses on the scale of the whole cell.

In this chapter we review a selection of theories on how mechanical material properties and growth processes interact to induce the onset of actin based motion.

PACS numbers: 87.17.Jj 87.15.Rn 82.39.-k 82.35.Pq 62.40.+i 81.40.Jj

I. INTRODUCTION

Most living cells are able to perform a directed motion, either by swimming in a liquid environment, by crawling on a solid support or by squeezing through a three-dimensional matrix of fibers.

The speed of swimming bacteria can reach up to $100 \mu\text{m s}^{-1}$, whereas eukaryotic cell crawling can be as fast as $1 \mu\text{m s}^{-1}$ (Ref. [17] and references therein). Given their size and speed, the motion of single cells is governed by viscous forces, not inertia, i.e. the Reynolds number $Re \ll 1$.

Unicellular organisms move in search of a food or light source. Intracellular pathogens like bacteria or viruses spread by exiting their host cell and entering a neighboring cell. Other simple organisms like the slime mold *Dictyostelium discoideum* migrate under unfavorable conditions, e.g. starvation, towards an aggregation center to form a multicellular organism.

Typically, in a multicellular organism not all cells are motile all the time but they can be mobilized by the appropriate stimuli. For example, the ability to move plays a crucial role during embryonic development, in wound healing and in the immune response. Additionally, cellular motility is a prerequisite for metastasis formation during cancer development

The biological realizations to produce a propulsive force are diverse. Most swimming cells, e.g. sperm cells or the bacterium *Escherichia coli*, use one or multiple beating flagella¹, respectively. In contrast, crawling cells and some intracellular pathogens advance by actin polymerization.

In this article we will present recent experiments and concepts to understand the latter mechanism, the production of forces in the advancing edge of crawling cells or for the propulsion of intracellular organelles, which is also of fundamental interest for the medical and engineering sciences.

The foundation of the research of cell motility as a distinct discipline were laid in the 1970's by the group around Michael Abercrombie [1]. He was the first to divide the motion of fibroblasts² into three phases, Extension - Adhesion - Contraction, which form the dogma of cellular motion as it is recognized today. In this mechanism, a slow movement ($\sim 1 \mu\text{m min}^{-1}$) is generated by the extension of flat membrane sheets, lamellipodia, into the direction of movement. The advancement of the membrane is accompanied by the formation of focal adhesions, contacts between the substratum, the cell membrane and actin stress fibers. Finally the cell rear retracts, accompanied by a deadhesion of the membrane from the substratum.

*Electronic address: kjohn@spectro.ujf-grenoble.fr

†Electronic address: cmisbah@spectro.ujf-grenoble.fr

¹ long cellular extensions

² most common cells of connective tissue in animals

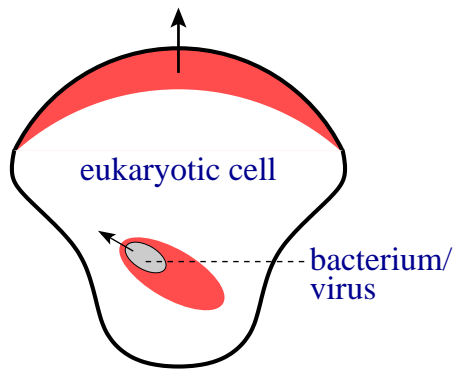


FIG. 1: Actin polymerizes into an elastic filament network (shaded in grey) at the leading edge of motile eukaryotic cells or at the outer surface of pathogens and organelles and induces cellular motion. The direction of motion is indicated by the black arrows.

However, there exist variations of this dogma. Fish keratocytes³ perform a rapid continuous motion ($\sim 10 \mu\text{m min}^{-1}$) with a constant shape. They almost seem to glide over the surface and form only transient focal contacts with the substratum with a much shorter lifetime than the focal adhesions formed in fibroblasts [3].

Another variant is the rapid motion ($\sim 10 \mu\text{m min}^{-1}$) of the slime mold *Dictyostelium discoideum*, which moves in an amoeboid fashion. During this amoeboid motion only non-specific contacts with the substratum are formed and actin stress fibers are absent [18].

Despite the various mechanisms, cell motion requires first of all the self-organization of the cell into an advancing and receding edge. This manifests itself by different molecular concentrations or activation levels of enzymes at the two poles. The polarization can be guided by external signals, e.g. chemical gradients or a variation in the mechanical properties of the support, but it might also arise in a homogeneous environment, after a transient mechanical perturbation of a stationary symmetric cell [60].

The three processes, extension, adhesion and contraction are coupled by sophisticated and complex mechanisms. However, it seems as if the process of front extension relies on a completely different machinery than that of adhesion and contraction and can be studied separately.

It had been known for a long time that on a cellular level, forces can be generated on the basis of muscle like proteins, i.e. actin and myosin, which is indeed responsible for the contraction of the cell rear [27]. However, more recently it was discovered that the protrusions at the leading edge as well as the motion of intracellular organelles [29] or pathogens, like the bacterium *Listeria monocytogenes* [53] or the *Vaccinia* virus [13], can be associated with the so-called actin polymerization machinery [52] as shown schematically in Fig. 1.

³ fish scale cells

The molecular basis and minimal ingredients of actin polymerization forces are now very well understood thanks to biomimetic experiments in the group of Marie-France Carlier [33]. However, the theoretical understanding of the physical mechanisms of polymerization process are still a matter of debate and shall be the main topic of this review.

In the first introductory part we will outline the biochemical basis of actin polymerization and present a selection of experimentally observed phenomena. Here we will shortly present the processes taking place at the leading edge of locomoting cells and then we will mainly rely on biomimetic experiments. In a second part we will present some theoretical concepts to interpret and understand the existing experiments. The list of presented models is by no means complete and rather represents a selection of the leading ideas. Here we will focus on the class of Brownian ratchet models and macroscopic models on symmetry-breaking.

II. EXPERIMENTAL OBSERVATIONS

A. Biochemistry of actin polymerization and organization of the leading edge of advancing cells

Actin is a small globular protein of 42 kDa present in all eukaryotic cells [51]. Under physiological conditions actin monomers (G-actin) polymerize into long helical filaments (F-actin). In a living organism these polymerization or depolymerization processes are tightly regulated. The literature on the dynamics of actin and the proteins which interact with actin is vast. As an introduction we would like to refer the reader to the comprehensive biochemical reviews by Pollard et. al. [46, 47] and Rafelski et al. [49] or the books by Bray [7] and Howard [26]. Due to the limited scope of this bookchapter we will just present the basic phenomena and common terminology associated with the actin polymerization machinery, which will allow the reader to understand the pertinent questions and concepts.

1. Actin polymerization in vitro

Under physiological conditions, i.e. at an ionic strength of $\sim 100 \text{ mM}$, monomeric actin polymerizes spontaneously into filaments. The filament growth process typically starts with a nucleation process, since actin dimers and trimers are unstable. Shortening or elongation of existing filaments occurs predominately via subunit addition or subtraction at the filament ends and not via filament breaking or annealing processes. Actin monomers at a concentration c may bind to a filament end with a rate $\sim k_+c$ and dissociate with a rate $\sim k_-$. In a stationary situation, i.e. zero net growth of the filament, one can write

$$0 = k_+c - k_- . \quad (1)$$

The concentration $c_c = k_-/k_+$ associated with this equilibrium is called critical concentration.

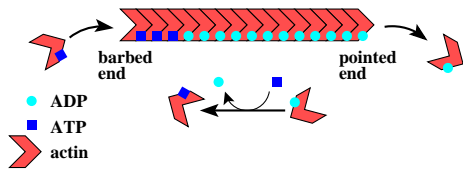


FIG. 2: Actin subunits treadmill through a filament. ATP-actin polymerizes at the barbed end, ATP hydrolyzes and ADP-actin depolymerizes at the pointed end. In the solution ATP is exchanged for ADP at the monomers.

G-actin has a structural polarity [25]. The same polarity is also found in actin filaments and can be visualized as an arrowhead pattern by decoration of filaments with myosin⁴. From this arrowhead pattern the two filament ends are referred to as pointed and barbed, respectively, as shown in Fig. 2.

In the presence of Mg-ATP the structural difference translates into a difference of the critical concentrations and rate constants between the barbed and pointed ends and causes a treadmilling of subunits through the filament.

Briefly, this phenomenon can be explained as follows (for details see Ref. [46]). Most actin monomers are bound to ATP (typically Mg-ATP). The critical concentration for this ATP bound species is about 6 times lower for the barbed end than for the pointed end. For ADP actin the critical concentrations are about the same for both ends but about ten times higher than for ATP actin at the barbed end. Therefore, in the steady state the ATP actin concentration is above the critical concentration of the barbed end and below the critical concentration of the pointed end. Polymerized actin subunits are still bound to ATP but in the course of time ATP hydrolyzes irreversibly into ADP+ P_i and, later on, the anorganic phosphate P_i dissociates from the filament with a half-time of several minutes. Consequently, ATP actin polymerizes at the barbed end, travels along the filament whereby ATP is hydrolyzed and finally ADP actin depolymerizes at the pointed end. Fig. 2 shows schematically the main key processes of the treadmilling cycle.

The process of irreversible ATP hydrolysis and P_i release (and subsequently the exchange $ADP \rightarrow ATP$ at the actin monomer in solution) keeps the system out of equilibrium and allows for a constant flux of monomers through the filament at constant filament length, which is called treadmilling and forms the base of cellular motility.

2. Proteins that regulate actin polymerization *in vivo*

In the living cell the actin polymerization machinery is tightly regulated by signalling processes. Many different factors interact with actin or participate in the regulation of this

polymerization machinery. In the following paragraphs we will only discuss the relevant factors which determine the actin architecture of the leading edge of advancing cells or the actin comets formed by intracellular pathogens and which seem to be crucial to generate motion.

First of all, most actin monomers are bound to so-called monomer binding proteins, e.g. Thymosin- β_4 and Profilin, and are thus not able to nucleate new filaments. But Profilin-ATP-actin complexes elongate existing filaments at the barbed end nearly as efficiently as ATP-actin.

Electron micrographs of the leading edge show a dense network of actin filaments linked to each other by Y junctions, where a new filament grows from an existing filament at a 70° angle. The distance between two crosslinks is of the order $\sim 20\text{--}30$ nm (in comparison, the persistence length of actin filaments is $15\ \mu\text{m}$ [42]). This Y junction is initiated by the interaction of the Wasp/Scar protein and the Arp2/3 complex, whereby Wasp/Scar is a membrane bound protein which incites the binding of the Arp2/3 complex to an existing filament, which in turn then serves as a nucleation point for a new filament.

Free barbed filament ends are quickly covered by so called capping proteins, thus limiting filament elongation to a zone near the plasma membrane. At the pointed filament end depolymerization takes place. This process can be accelerated by a protein complex called ADF/cofilin, which is able to sever old filaments containing ADP actin subunits. These filament fragments are then depolymerizing rapidly. Besides Arp2/3 there exist other types of filament nucleators, called formins. In the presence of profilin and ADF/cofilin they seem to favor the growth and bundling of several actin filaments into cables [38], present in spike-like membrane extensions, called filopodia. In this chapter we will limit ourselves to actin networks produced by the Arp2/3 complex.

The above outlined process of polymerization at the membrane/actin network interface and depolymerization far away from the membrane provides the mechanism for pushing the membrane into the direction of movement. However, little is known about the mechanical properties of such filament networks and recent experiments indicate that the loading history determines the growth velocity of the network [43].

Certain bacteria invade other living cells and hijack the actin polymerization machinery of their host cells to propel themselves forward. They carry a protein on their outer surface (e.g. ActA for *Listeria monocytogenes*), which adopts the same function as the Wasp/Scar protein in the membrane of eukaryotes: it triggers the polymerization of an Arp2/3 crosslinked network at the outer bacterial surface. This actin network typically develops asymmetrically only at one side of the bacterium thus pushing the bacterium in the other direction.

A similar mechanism might also be responsible for the motion of endocytic vesicles in living cells (see [29] and references therein).

To summarize the growth processes and the resulting architecture of the actin system at the leading edge: close to the cell membrane containing an activating enzyme (e.g. Wasp or ActA), actin polymerizes into a dense crosslinked filament

⁴ Myosin molecules bind to each actin subunit in the filament in an oriented fashion, leading to a typical pattern along the filament, which looks like a series of arrowheads in an electron micrograph. For details see Ref. [7].

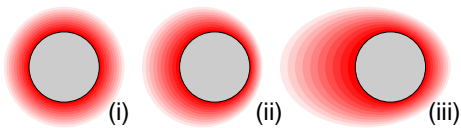


FIG. 3: Schematic view of the evolution of an actin gel (shades of red) around a bead (grey) as described in the text with (i) a symmetric growth, (ii) the symmetry-breaking, and finally (iii) the comet formation.

network, which extends several μm into the cell and where fast polymerizing barbed ends are oriented towards the membrane. Polymerization is restricted to a narrow zone close to the membrane since free barbed ends are rapidly blocked by capping proteins. Free pointed ends which are far away from the membrane are depolymerizing. These out of equilibrium growth processes driven by the irreversible hydrolysis of ATP lead to the extension of membrane protrusions or propel bacteria forward.

B. Biomimetic experiments

1. General observations

The minimal set of biochemical ingredients to induce actin driven motion have been identified about ten years ago [33]. At the same time actin driven motion has been successfully reconstituted *in vitro* by replacing the bacterium by mimetic objects, e.g. beads [11, 41, 62], vesicles [23, 35, 56] or droplets [6].

In these experiments objects (hard, soft, fluid) coated with either ActA or Wasp/Scar proteins are added to a solution containing ATP actin, capping protein and a few well defined regulatory proteins. With this design, actin polymerizes predominantly at the surface of the object, i.e. the internal interface, and depolymerizes at the interface between the network and the solution, i.e. the external interface.

After an initial phase (i), where polymerization occurs symmetrically around the object, the symmetry is broken and the actin cloud starts to grow asymmetrically (ii). In later stages an actin comet develops (iii), and the object starts to move with velocities up to $0.1 \mu\text{m s}^{-1}$. A schematic representation of the three phases of the actin cloud evolution is shown in Fig. 3. Interestingly the mode of movement depends on the surface parameters of the object. Depending on the conditions one can observe a continuous motion or a saltatory motion, where the object undergoes stop-and-go cycles [5, 14, 31, 55], which is also reflected by variations in the actin density in the comet.

The network grown around these biomimetic objects has elastic properties with a Young's modulus of 10^3 - 10^4 Pa [20, 36] and is often referred to as an actin gel.

The actin filaments interact, at least transiently, with the activating enzyme bound to or adsorbed on the objects surface, e.g. the stress to detach an actin comet from a bead has been estimated to be of the order of $\sim 100 \text{ pN } \mu\text{m}^{-2}$ [36], whereby the adsorbed activating enzyme stays on the bead.

Interestingly, in the same experimental setup actin comets under compression appeared to be hollow.

In regime of continuous motion the bead velocity is not affected by the viscosity of the medium (over five orders of magnitude). This raises the question of the dissipative force, which is obviously not the Stokes force on the object (about 1 fN for a bead of $1 \mu\text{m}$ radius moving with a velocity of $1 \mu\text{m min}^{-1}$ in a standard motility assay). In contrast, the stalling force for the growing actin tail is a few nN [36, 48]). Several studies indicate that friction between the actin gel and the propelled object is the major source of dissipation [19, 61]. This would support the hypothesis, that the saltatory bead or vesicle motion is the result of a stick-slip motion, where a certain critical force has to be overcome to rupture bead-gel bonds and to displace the object with respect to the gel [4, 19].

2. Symmetry-breaking

Biomimetic experiments are not only an effective tool to study the generation of motion by polymerization but they have also revealed a spontaneous symmetry-breaking instability in the growing actin network (transition from (i) to (ii) in Fig. 3), whose consequences *in vivo* are not clear and whose nature is still a subject of debate in the literature.

Even though, as often argued by biologists, a symmetry-breaking does not play a role in bacterial systems, since the ActA proteins are distributed asymmetrically around the bacterium due to a previous cell division, the instability is a powerful tool to study the coupling mechanisms between actin polymerization and mechanical stresses.

So far there seems to be a consensus in the literature, that mechanical stresses build up in the actin network due to growth, since new monomers are inserted at the internal curved interface and push older network layers away from the object. In a symmetric situation one expects therefore high tangential stresses at the external actin/solution interface and high normal stresses at the internal object/actin interface. Then the symmetry-breaking is driven by a release of elastic stresses in the actin gel, either by an asymmetric polymerization/depolymerization or by a fracture at the external gel interface, whereby the two mechanisms are difficult to distinguish.

There seem to exist subtle differences in the nature of the symmetry-breaking for hard [11, 41, 62] and soft objects [23, 35, 56], as was demonstrated in a more recent study [14]. In fluorescence labeling experiments it was shown that for soft objects (vesicles) the symmetry is broken at the internal gel interface, i.e. polymerization is considerably slowed down on one side of the vesicle, such that an actin tail develops at the opposite side. In contrast, for hard beads the symmetry is broken at the external (depolymerizing) gel interface, whereby some authors suggest, that the filament network is ruptured due to an accumulation of tangential stresses [58], whereas theoretical models indicate that a local stress dependent depolymerization is sufficient to induce a symmetry-breaking [28, 50]. Note however, that actin driven motion itself does not require the polymerization at curved surfaces, as has been

demonstrated theoretically [12].

Furthermore, the mechanical properties of the biomimetic object has an effect on the mode selection of the instability. Whereas for soft objects only instabilities, which produce one single actin tail, have been reported, there are observations of higher order instabilities for hard spheres depending on the experimental conditions [14]. Therefore, the boundary conditions at the internal gel interface seem to be crucial for the mode selection.

III. THEORETICAL APPROACHES

Two types of theoretical concepts, how polymerization processes transform biochemical into mechanical energy, have been developing in parallel over the past 15 years.

The first type of concept, called ‘‘Brownian ratchet models’’ was introduced by Peskin et al. [44]. Its major postulate is that polymerization processes (e.g. actin polymerization) are able to rectify the Brownian motion and can thus induce motion. Brownian ratchet models describe microscopically the polymerization of actin filaments in the presence of an obstacle. Although very consuming in terms of computational efforts, Brownian ratchet models allow for the incorporation of a very detailed description of the kinetics of the polymerization machinery. They provide ingenious tools to study the complex phenomena which have been observed in biomimetic experiments.

The second type of concept, we shall refer to it as macroscopic concept, does not focus so much on the dynamics of the single filament, but rather considers the actin filament network as a continuous elastic body under growth, where the growth dynamics is driven by a thermodynamic force, the chemical potential. These coarse-grained models emphasize the global stress distribution in the filament network and the nonlocal aspect of elasticity, while neglecting the details of the polymerization process. Nevertheless, they are more suitable to describe and understand the symmetry-breaking in actin gels around spherical objects in terms of simple physical ingredients.

The ideal multiscale model would combine both concepts and use the global stress distribution as an input for the complex polymerization kinetics at the free interfaces.

In the following section we will briefly review the two concepts. In the first subsection on Brownian ratchet we will mainly discuss Refs. [16, 21] as they provide, from our point of view, the most advanced description for the polymerization dynamics close to the obstacle. In the second subsection on macroscopic models we will shortly outline and discuss the major drawbacks of Refs. [50] and [28] and then give a perspective, how these problems can be solved using homogenization techniques.

A. Brownian ratchet models

1. General concept

As mentioned above, the idea of a Brownian ratchet model for polymerization forces in biological system was introduced by Peskin and coworkers [44]. This work explored the rectification of the Brownian motion of a particle by the intercalation of new monomers at the interspace between a filament tip and the obstacle, which gives an ideal ratchet velocity v of

$$v = \frac{2D}{\delta}, \quad (2)$$

where D denotes the diffusion coefficient of the obstacle and δ the size of a monomer. However, later on it was shown, that the actin driven motion was relatively independent of the obstacle size [24] and independent of the viscosity of the medium over several orders of magnitude [61], i.e. independent of D . Therefore, the concept of Brownian ratchets was generalized to ‘‘elastic Brownian ratchets’’, where the tips of polymerizing filaments undergo fluctuations, which induce a propulsive force on the obstacle [39, 59] and to ‘‘tethered ratchets’’ [40], which involves also the transient attachment of fluctuating filament tips to the obstacle. Typically in this description the polymerization rate constant k_p is weighted by the load f using Kramers theory

$$k_p = k_p^{max} e^{-f\delta/k_B T}, \quad (3)$$

where k_p^{max} is the rate constant at zero load, δ represents the gap size to intercalate a monomer, k_B and T denote the Boltzmann constant and the absolute temperature, respectively.

The general framework has been used to quantitatively model the steady motion of flat objects [12], lamellipodia and bacterial motion [39, 40]. However, stochastic effects in the number of polarizing filaments were necessary to break the symmetry in a spherical gel around a bead homogeneously covered by ActA or Wasp, whereas the global elastic stress distribution due to filament crosslinking was neglected [40, 59].

Other attempts to model biomimetic motility quantitatively by explicitly modelling the filament dynamics in the actin tail succeeded in obtaining the crossover from a continuous to a hopping motion [2, 8]. However, the velocity oscillations were on a time scale of ms with stepsizes of a few nm, as opposed to the experimental oscillations on the scale of several min with stepsizes on the μm scale [5, 14, 31, 55].

More recently, the tethered ratchet model of Mogilner et al. [40] was submitted to a more rigorous treatment concerning the polymer physics of the filament brush close to the obstacle [16, 21]. Further away from the obstacle the cross-linked gel is advancing with a so-called grafting speed (force dependent and coupled to the brush length). In the following we will highlight the basic features of this model, since it quantitatively reproduced velocity oscillations.

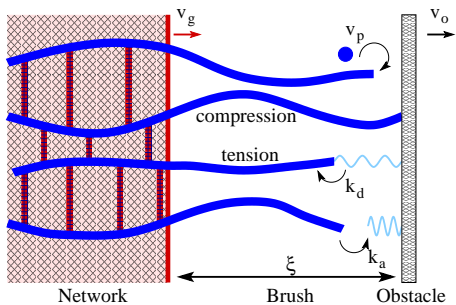


FIG. 4: Schematic representation of the elastic ratchet model as explained in the text. Filaments are anchored with one end into a cross-linked network forming an actin-gel and oriented with the other end against an obstacle. Adapted from Refs. [16, 21].

2. A quantitative model for velocity oscillation in actin-based motility

As mentioned previously, the motion of a mutant form of the bacterium *Listeria* (with a mutation in the ActA protein) is oscillatory and shows remarkable temporal patterns [19, 31]: the bacteria move very slowly during 30 to 100 s, jump forward during a few seconds and then slow down again abruptly. Such a periodic behavior, consisting of long intervals of a slowly changing dynamics that alternate with short periods of very fast transition, are found in several chemical and biological systems and are known as relaxation oscillations [30].

Gholami et al. [21] and Enculescu et al. [16] have developed a microscopic model based on the concept of tethered elastic ratchets for actin-based motility. Their model consists of a brush of growing actin filaments close to an object (the bacterium) and describes the generation of forces and consequently the propulsion of the object.

Briefly, the model considers the case of fluctuating filaments close to an obstacle. Filaments may attach to the obstacle with a rate constant k_a and detach from the obstacle with a force dependent rate constant k_d , resulting in two distributions of populations of filaments, i.e. of attached and detached n_a and n_d , respectively. Opposite to the obstacle the filament ends are anchored in a cross-linked network, the actin gel. Detached filaments polymerize with a load dependent velocity v_p . The distance between the grafting point, i.e. the interface between the network and the polymer brush, and the obstacle is denoted by ξ . The filaments are characterized by their free contour lengths l . One of the crucial ingredients of the model is, that the grafting point is advancing in the direction of the obstacle with a so called grafting velocity v_g , which depends on the free contour lengths of the polymers by

$$v_g(l) = v_g^{max} \tanh(l/\bar{l}), \quad (4)$$

where \bar{l} denotes a characteristic width of boundary between the crosslinked network and the filament brush.

Attached and detached filaments exert entropic forces [22] on the obstacle, $F_a(l, \xi)$ and $F_d(l, \xi)$, respectively, which lead to the propulsion of the object with an effective friction coefficient ζ .

The load dependence of the kinetic rate constants is again included using a Kramers type expression [see Eq. (3)], i.e.

$$k_d(F_a) = k_d^0 \exp(-\delta F_a/k_B T) \quad (5)$$

for the detachment and

$$v_p(l) = v_p^{max} \exp(-\delta F_d/k_B T) \quad (6)$$

for the polymerization speed.

The full evolution of the length distributions of the two filament populations $n_a(l, t)$ and $n_d(l, t)$ is described by advection-reaction equations. However, it is shown that the two distributions contract rapidly on the scale of 10^{-2} s into monodisperse distributions $N_a = n_a(t)\delta(l - l_a(t))$ and $N_d = n_d(t)\delta(l - l_d(t))$ localized at l_a and l_d for attached and detached filaments, respectively. Therefore, the dynamics of the system can be simplified to four ordinary differential equations for the evolution of the free contour lengths $l_a(t)$ and $l_d(t)$, respectively, the number of attached filaments $n_a(t)$ (the total number of filaments N is constant and therefore $n_d(t) = N - n_a(t)$) and the distance $\xi(t)$ between the obstacle and the grafting point.

The solution behavior of this system of equations has been analyzed numerically depending on the maximal grafting speed v_g^{max} and the rate constant for the attachment of filaments k_a . Fortunately, most other model parameters are known experimentally. The model displays two different dynamical regimes: steady and oscillatory motion, whereby the oscillatory regime is robust against changes in the parameters. The oscillations occur on the time scale of min and produce jumps of the obstacle displacement in the μm range and resemble very much relaxation oscillations.

A deeper analysis of the solutions suggests, that the oscillations arise from a so called push-pull mechanism, i.e. a competition between pulling and pushing forces acting on the obstacle. In this mechanism, a long pull phase, where most of the filaments are attached to the obstacle and polymerization stalls, alternates with a short push phase, where most filaments are detached and polymerize rapidly. In the pull phase the grafting velocity v_g is higher than the polymerization speed v_p , and the magnitude of the forces on the obstacle increases due to their dependence on ξ , l_a , and l_d . At a certain point, in the pushing phase, the pushing forces outweigh the pulling forces and cause an avalanche like detachment of filaments and the obstacle ‘‘hops’’ forward, lowering the load on the detached filaments, which start to polymerize rapidly and thus $v_g < v_p$. Meanwhile free filaments start to attach to the obstacle and increase the pulling force, i.e. the obstacle slows down. Free filaments start to buckle, the polymerization stalls and the cycle reenters the pulling phase.

Obviously, this complex cycle arises from the subtle interplay between pushing and pulling forces on the one hand and the grafting and polymerization velocities on the other hand. It would be an interesting task, to explore the parameter space a little bit further and identify the absolutely necessary ingredients to find oscillations in the push-pull mechanism.

Besides steady and oscillatory motion the model also yields bistable and excitable behavior, which might lead to the reinterpretation of previous experiments and is reminiscent of the

behavior caused by nonlinear friction in a variety of systems with a complex surface chemistry [57]. Another aspect for future work is to couple the microscopic dynamics of the filament brush to the bulk mechanics of the cross-linked gel.

B. Macroscopic models

While microscopic models give a detailed description of the polymerization and cross-linking dynamics, macroscopic models are more concerned about the global stress distribution in the gel, but adopt a more general formulation for the interface dynamics. In the following we will shortly introduce and discuss the essence of three simple models, i.e. by Lee et al. [32], Sekimoto et al. [50], and John et al. [28], describing the symmetry-breaking in an actin gel around a solid bead. We will conclude this section with the discussion of a more advanced mechanical model using homogenization techniques proposed by Caillerie et al. [10].

1. A phenomenological model of symmetry-breaking

As an introduction we will present the problem of symmetry-breaking from a purely phenomenological point of view as proposed by Lee et al. [32]. If a bead moves, it is natural to assume that a force is applied on the bead, probably due to deformed filaments that releases stress on the bead. Let $g(\mathbf{r}, t)$ denote the force per unit area in the normal direction that is exerted on the bead, which could be e.g. a function of the local actin concentration. The total force on the bead is given by $\mathbf{F} = \int g(\mathbf{r}, t) \mathbf{n} dA$, with \mathbf{n} being the unit normal vector on the bead. The velocity of the bead is related to the total force via a linear relation

$$\mathbf{v} = \xi \mathbf{F} = \xi \int g(\mathbf{r}, t) \mathbf{n} dA, \quad (7)$$

where ξ is a dissipative coefficient, taken to be scalar for simplicity (it is necessarily so for a sphere in a Newtonian fluid).

It is then assumed that the rate of change of $g(\mathbf{r}, t)$ is a local function of the bead velocity \mathbf{v} , and that there is a feed back of the motion on the force g : faster motion is associated with a decrease of polymerization in the front and an increase of polymerization at the rear, and hence has an impact on g . Under the assumption of analyticity, the evolution of g can be written as

$$\partial_t g = -g - g^2 - cg^3 + a\mathbf{v} \cdot \mathbf{n} + b g \mathbf{v} \cdot \mathbf{n}, \quad (8)$$

with $c > 0$ in order to ensure stability of the homogeneous stationary state $g = 0$. The signs of a and b are left arbitrary for the moment. Eqs. (8) and (7) constitute a complete set that can be solved numerically or analytically using a perturbation ansatz as will be outlined in the following.

It is a simple matter to see that the set [Eqs. (8) and (7)] admits the fixed point $g = \mathbf{v} = 0$. By superposing small perturbations on this solution, reporting into the above set, and expanding up to linear order in the perturbations, one finds

that the fixed point is unstable for $a > 3/\xi \equiv a_c$ and stable otherwise. If motion takes place then this means that a symmetry-breaking has occurred, and thus the local force g has lost the spherical symmetry. More precisely by expanding g in spherical harmonics, $g = \sum_{\ell m} g_{\ell m} Y_{\ell m}(\theta, \phi)$, and reporting into (8) by assuming a direction of motion, say along oz , one finds to leading order

$$\partial_t g_{\ell m} = \left[1 - \frac{a}{a_c} \delta_{\ell 1} \right] g_{\ell m} + \dots \quad (9)$$

whereby the “...” refer to nonlinear terms. Integration of other harmonics than the mode $\ell = 1$ in (7) vanishes exactly due to symmetry. Beyond the symmetry-breaking bifurcation for $a > 3/\xi$ the perturbations grow exponentially in time, and nonlinear terms are needed. Since only the mode $\ell = 1$ is excited, the other modes are treated as adiabatically enslaved to it (at least in the vicinity of the threshold). The following analysis consists in expanding the solution for higher order terms and expressing the amplitudes of the higher harmonics in terms of the amplitude of the first order mode. Once g has been replaced by \mathbf{v} from (7) and inserted into (8) a closed equation for \mathbf{v} (which is simpler to assess experimentally than g) is obtained [32]

$$\partial_t \mathbf{v} = \epsilon \mathbf{v} + \frac{27}{5\xi^2} \left[\left(\frac{\xi b}{3} - 1 \right) + \left(\frac{\xi b}{3} - 2 \right) - c \right] \mathbf{v}^3 + u \mathbf{v}^5. \quad (10)$$

$\epsilon \equiv (1 - a/a_c)$ is a small parameter (expressing the fact that we focus on the instability threshold), and we have used the convention $\mathbf{v}^3 = v^2 \mathbf{v}$, and so on. The expression of u in terms of the coefficients a , b , c , and ξ is not shown here. However, it is reported in [32] that u is negative in the considered parameter space. The amplitude equation (10) serves to discuss the phenomenology of the motion, that we will briefly summarize here and which is shown schematically for the $b - a$ -parameter plane in Fig. 5.

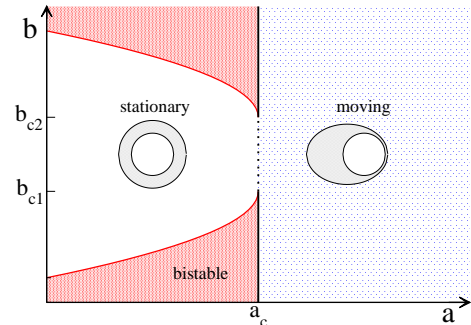


FIG. 5: Phase diagram arising from the analysis of Eq. (10). The transition between the stationary (white region) and moving (light shaded region) state occurs at $a = a_c$. For $b_{c1} < b < b_{c2}$ the bifurcation is supercritical. In the dark shaded region there coexist two solutions $\mathbf{v} = 0$ and $\mathbf{v} = \text{const} \neq 0$ which are linearly stable. Adapted from Ref. [32].

If the coefficient of the cubic term is negative, then a continuous transition from the symmetric (motionless) to the asymmetric (moving) state occurs at $\epsilon = 0$, i.e. the bifurcation is

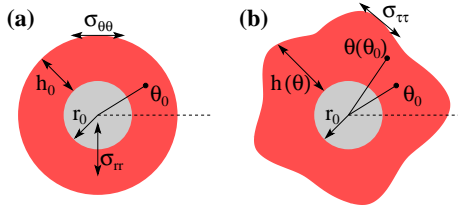


FIG. 6: Schematic view of a bead surrounded by an elastic gel, showing several definitions as explained in the text. Shown is a symmetric gel (left) and an asymmetric gel (right). In the latter case the tensile stress is rather generally denoted by $\sigma_{\tau\tau}$ with τ designating the tangent direction.

supercritical (an analogue of a second order transition). This happens for a certain range of the product ξb and by fixing c to unity for definiteness. For a certain range of the product ξb the cubic coefficient changes sign, a signature of a sub-critical bifurcation (an analogue of a first order transition). This is known to lead to multistability: in a certain parameter range for $\epsilon < 0$ there coexist two solutions: $\mathbf{v} = 0$ and $\mathbf{v} = \text{const}$, both solutions being locally stable, i.e. stable with respect to small perturbations. One may think that the system may switch back and forth between the two solutions.

Several remarks are in order. (i) The above discussion is fully phenomenological, and actually Eq. (10) could have been written directly. However, the derivation given in [32] has a certain merit with regard to the description of the general laws behind the motion, and the feedback mechanism. (ii) The coefficients are certainly complicated functions of experimental parameters, and a microscopic model is needed in order to relate phenomenological and experimental parameters. (iii) The origin of the forces acting on the bead and the subsequent generation of motion in this model is not clear. We will come back to this vital question in the final conclusions.

2. The role of tensile stress during the symmetry-breaking in actin gels

A first physical macroscopic model including elasticity has been put forward by Sekimoto et al. [50] in order to explain the birth of the symmetry-breaking of an initially symmetric gel layer growing on a spherical or cylindrical object. The crux of their analysis is that the gel that has been formed is being continuously pushed outwards due to the arrival of new monomers at the bead. This is supposed to lead to large lateral stresses on the outer gel interface. A schematic representation of the model is shown in Fig. 6. In the following we outline the model in a cylindrical geometry. If $\sigma_{\theta\theta}$ designates the tangential stress, and if the gel layer is axisymmetric, it is postulated that

$$\sigma_{\theta\theta} = E \frac{r - r_0}{r_0}, \quad (11)$$

where E is the Young modulus. At $r = r_0$ (the bead radius) the tensile stress vanishes, expressing the assumption

that the gel layers are added unstretched at the bead surface. If h denotes the total gel thickness, one can write for the tensile stress at the external gel surface $\sigma_{\theta\theta}|_{r=r_0+h} = E \frac{h}{r_0}$. The external surface of the gel is not subject to a force, so that both the tangential and normal forces must vanish, i.e. $\sigma_{r\theta}|_{r=r_0+h} = \sigma_{rr}|_{r=r_0+h} = 0$. The tangential force is also zero at the bead surface, $\sigma_{r\theta}|_{r=r_0}$. For a symmetric gel the shear stress vanishes everywhere in the gel. If a non zero tensile stress exists [Eq. (11)], the mechanical equilibrium in the bulk, i.e.

$$\text{div}(\sigma) = 0 \quad (12)$$

provides the following relation between the tensile and radial stress distribution, $\sigma_{\theta\theta}$ and σ_{rr} ,

$$\sigma_{rr} = \frac{E}{2r_0 r} [(r - r_0)^2 - h^2]. \quad (13)$$

The gel may grow because of a gain in polymerization energy at the bead surface. This growth takes place at a certain price: the higher the thickness of the gel is, the larger is the stored elastic energy. Therefore, one expects the growth to stop at a certain equilibrium thickness h_0 . The following growth kinetic relation has been suggested [50]

$$\partial_t h = k_p e^{c_p \sigma_{rr}|_{r=r_0}} - k_d e^{c_d \sigma_{\theta\theta}|_{r=r_0+h}} \quad (14)$$

where k_p , k_d , c_p , c_d are positive constants. The first term, which is positive, accounts for the polymerization at the bead, while the second one, which is negative, refers to depolymerization at the external surface. Note that on the one hand $\sigma_{rr}|_{r=r_0} = -Eh^2/(2r_0^2) < 0$, and thus stress penalizes polymerization and acts against gain in chemical bonds at the bead. On the other hand $\sigma_{\theta\theta}|_{r=r_0+h} > 0$ and this causes the depolymerization to increase with the gel thickness, since $\sigma_{\theta\theta}|_{r=r_0+h}$ increases with h . Setting $\partial_t h = 0$ provides us with the steady state thickness h_0 as a function of other parameters. One straightforwardly finds

$$\frac{c_p}{c_d} \left(\frac{h_0}{r_0}\right)^2 + \frac{h_0}{r_0} - \frac{2}{c_d E} \ln\left(\frac{k_p}{k_d}\right) = 0. \quad (15)$$

A steady solution exists as long as $k_p/k_d > 1$. It can easily be checked that the steady solution h_0 is stable with respect to a homogeneous, i.e. axisymmetric, increase or decrease of h_0 . One further sees that h_0 is a linear function of r_0 , since only the ratio h_0/r_0 enters the above equation. This seems to be in good agreement with experimental observations [41].

Let us now discuss the linear stability analysis of the steady solution with respect to perturbations that break the circular symmetry. In a cylindrical geometry the eigenmodes are $\sim e^{im\theta_0}$ (or $\cos(m\theta_0)$ in real variables) where θ_0 is the angular variable shown in Fig. 6, and m is an integer. Because the equations are autonomous with respect to time, all the eigenmodes can be written as $\sim e^{\beta t}$, where β is the amplification or attenuation rate of the perturbation that must be determined from the model equations. We set for the perturbed thickness

$$h(\theta_0) = h_0[1 + \epsilon_m(t) \cos(m\theta_0)]. \quad (16)$$

ϵ_m is a small, time-dependent quantity that justifies the linear stability analysis. The stress field inside the gel will thus be parametrized by the function $h(\theta_0)$. The linear analysis now consists in (i) solving the stress field in the gel with the appropriate boundary conditions, and (ii) using the kinetic relation (14) to obtain the dispersion relation $\beta = f(m, p)$, where p is an abbreviation for all the physical and geometrical parameters that enter into the equation.

In order to solve for the elastic field, one needs to specify a constitutive law. Unlike in the two models [10, 28] we will discuss in the following sections, where a constitutive law is used by evoking basic continuum mechanics concepts, the Sekimoto et al. model [50] is based on an extension of the postulate represented by Eq. (11) to a modulated thickness $h(\theta_0)$. The basic ingredient of their analysis is to introduce an unknown function $\theta(\theta_0)$ such that a material point of the gel which is originally located at θ_0 in an undeformed reference state is moved to a new position $\theta(\theta_0)$ upon deformation. Then the elongation ratio $(r - r_0)/r_0$ is replaced by $(rd\theta(\theta_0) - r_0d\theta_0)/(r_0d\theta_0)$ so that the tensile stress takes the form

$$\sigma_{\theta\theta} = E \left[\frac{r}{r_0} \frac{d\theta(\theta_0)}{d\theta_0} - 1 \right]. \quad (17)$$

By using the equilibrium balance condition Eq. (12) and neglecting the shear stress (for a discussion of this assumption see Ref. [50]) one can again find a relation between σ_{rr} and $\sigma_{\theta\theta}$. By defining

$$T \equiv \int_{r_0}^{r_0+h} \sigma_{\theta\theta} dr \quad (18)$$

one deduces that

$$\sigma_{rr}|_{r=r_0} = -\frac{T}{r_0}, \quad (19)$$

since only this quantity enters the kinetic relation (14) that is needed for the derivation of the dispersion relation. Recall also, that $\sigma_{rr}|_{r=r_0+h} = 0$ to linear order in the perturbation ϵ_m . Upon using (17) the integral (18) leads to

$$T = E \left[\left(h(\theta_0) + \frac{h(\theta_0)^2}{2r_0} \right) \frac{d\theta(\theta_0)}{d\theta_0} - h(\theta_0) \right] \quad (20)$$

Additionally, Eq. (12) yields, under the assumption of zero shear stress, $\partial_\theta T = 0$, that is T is independent of θ . This condition provides a relation between $\theta(\theta_0)$ and $h(\theta_0)$. Upon using $\int_0^{2\pi} \frac{d\theta(\theta_0)}{d\theta_0} d\theta_0 = 2\pi$, one can express T as a function of an integral $\int_0^{2\pi} F(h(\theta_0)) d\theta_0$ where only $h(\theta_0)$ enters (F is given by Eq. (D5) of Ref. [50]). Plugging this relation into (20) provides a relation between $d\theta/d\theta_0$ and $h(\theta_0)$, and substituting h by Eq. (16) $\sigma_{\theta\theta}|_{r=r_0+h}$ and $\sigma_{rr}|_{r=r_0}$ can be deduced to first order in ϵ_m . After some algebraic manipulations the dispersion relation is obtained

$$\beta = \frac{\Omega_m k_d}{r_0}, \quad (21)$$

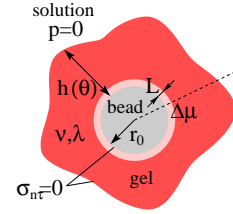


FIG. 7: Schematic view of a bead surrounded by an elastic gel, showing also several definitions of Ref. [28] as explained in the text.

where

$$\Omega_m = c_d E e^{c_d E \bar{h}_0} \frac{\bar{h}_0}{h_0 + 2} \quad (22)$$

and where we have set $h_0/r_0 \equiv \bar{h}_0$. β is positive, meaning that the perturbation grows exponentially with time: the symmetric gel layer is thus unstable. Surprisingly, the dispersion relation does not depend on m (since Ω_m does not). Consequently, all wavenumbers have the same growth rate. Thus, the linear stability analysis does not select a typical mode m (like the fastest growing mode) for the instability.

3. A nonlinear study on symmetry-breaking in actin gels

Unlike the previous model where a tensile stress distribution is *a priori* postulated, the idea of the model proposed by John et al. [28] is to treat the actin gel as an elastic continuum in the framework of a linear theory, and to formulate a simple kinetic relation expressing growth (or polymerization), different from Eq. (14).

The model considers a bead (radius r_0) surrounded by a growing elastic actin gel (radius $r_0 + h$) as shown in Fig. 7. The gel is stressed by a small molecular displacement L in normal direction at the bead/gel interface, i.e.

$$u_r|_{r=r_0} = L, \quad (23)$$

where u_r denotes the radial component of the displacement. This choice is motivated by the microscopic picture, that for the addition of monomers, enzymes facilitate a molecular displacement L at the bead/gel interface. This displacement is the source of stress. The bead/gel interface as well as the external gel surface is shear free and the normal stress at the external surface is set to zero⁵. No condition is imposed on the normal stress component at the bead, since there a displacement is imposed instead. The boundary conditions on the stress are thus

$$\begin{aligned} \sigma_{n\tau} &\equiv n_i \sigma_{ij} \tau_j |_{r=r_0, r=r_0+h} = 0 \\ \sigma_{nn} &\equiv n_i \sigma_{ij} n_j |_{r=r_0+h} = 0, \end{aligned} \quad (24)$$

⁵ Actually it can be set to $-p$, where p denotes the liquid pressure, but this contribution is quite small.

where n_i and τ_i are the i th component of the unit normal and tangent vector of the surface under consideration (bead or external gel surface).

The stress distribution in the gel is obtained then by solving the Lamé equation for the displacement field

$$\nabla^2 \mathbf{u} + \frac{1}{1-2s} \nabla(\nabla \cdot \mathbf{u}) = 0, \quad (25)$$

where s is the Poisson ratio. The stress is related to the displacement \mathbf{u} by Hooke's law

$$\sigma_{ij} = 2\nu\epsilon_{ij} + \lambda\epsilon_{kk}\delta_{ij}, \quad (26)$$

where $\epsilon_{ij} = (\partial_i u_j + \partial_j u_i)/2$ is the strain tensor, and λ and ν are the Lamé coefficients which are related to the Young modulus E and s (for an isotropic material there are only two independent elastic parameters).

Eqs. (23) - (25) represent a complete set that allows to determine, the stress and displacement fields in the gel. Note that, despite the fact that the bulk equations are linear, the problem acquires a nonlinear character via the geometry of the external gel boundary. Indeed if we fix a certain arbitrary geometry $h(\theta)$, then the stress and displacement will be a nonlinear function of h . The calculation can be handled analytically for a symmetric gel as well as in the linear stability analysis [28]. Beyond a linear analysis, a numerical study has been performed and will be briefly discussed below.

Once the mechanical problem is solved, one needs to compute the cost in elastic energy per unit mass for inserting a monomer on the bead/gel interface, i.e. the chemical potential difference. For the sake of simplicity we focus on the case of an inert external gel surface, i.e. neither polymerization nor depolymerization takes place at the external interface. We assume that insertion of a monomer at the bead results in a displacement of the external gel surface in the radial direction proportional to the chemical potential change at the bead. We will critically assess this assumption in the next section on homogenization models.

One may then write a kinetic relation of the shape evolution of the gel envelope

$$\partial_t h = -M\Delta\mu, \quad (27)$$

where M denotes a mobility and $\Delta\mu$ the difference in the chemical potential between a volume element in the gel and in solution at the internal interface. Here we assume that the mobility is associated with the polymerization/depolymerization kinetics, which constitutes the prevailing dissipation mechanism. The chemical potential is composed of a contribution due to the gain in polymerization (denoted as $\Delta\mu_p < 0$) and an elastic part [28]

$$\Delta\mu = \Delta\mu_p + \nu u_{ij} u_{ij} + \frac{\lambda}{2} u_{kk}^2 - \sigma_{nn}(1 + u_{kk}) \quad (28)$$

Note that (27) differs from (14) not only by the presence of the exponential function (which can be linearized since the stress energy is always small in comparison to the thermal excitation energy; hidden in the constant c_p), but most importantly by the

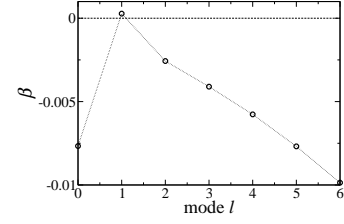


FIG. 8: The dispersion relation as a function of the mode l obtained from the linear stability analysis of the John et al. model [28]. The fastest growing mode corresponds to $l = 1$.

stress combination. Eq. (14) contains only a linear form and no quadratic forms as in Eq. (28). Here, the quadratic form is essential for the mode selection leading to a comet formation, as will be described below.

The stress problem Eqs. (23)-(25) can easily be solved analytically for a spherical geometry (axisymmetric growth). Upon setting $\partial_t h = 0$ in Eq. (27) one finds a steady solution with a gel thickness h_0 obeying [28]

$$h_0 = \left[\left(\frac{2E\alpha - (1-2s)\Delta\mu_p}{2E\alpha + (1+s)\Delta\mu_p} \right)^{1/3} - 1 \right] r_0, \quad (29)$$

where $\alpha = L/r_0$. This solution exists for $2E\alpha/(1+s) \geq -\Delta\mu_p$: elasticity acts against monomer addition, so that the gel stops growing at that thickness. In the opposite limit growth continues without bound. Both situations have been observed experimentally [45], however in the latter case growth stopped due to monomer depletion at the bead/gel interface.

The linear stability analysis of the symmetric case can be performed analytically (by decomposing the stress and the shape evolution into spherical harmonics $Y_{\ell m}$). The dispersion relation $\beta(\ell)$ is presented in Fig. 8. The basic result is that a symmetric shape is unstable against symmetry breaking [28]. Interestingly the mode which corresponds to a translation of the external surface with respect to the bead is the most unstable⁶. This translation motion is similar to that shown in Fig. 9 (b). For this instability the quadratic terms in Eq. (28) play a crucial role, since considering only the linear terms leads to a stable symmetric solution, with a zero growth rate for the translational mode.

In order to ascertain the subsequent evolution of the external boundary (i.e. in the fully nonlinear regime), a full numerical analysis has been performed [28]. The set of mechanical equations (23) - (25), and the growth kinetics (27) have been cast into a phase-field approach, which has now become a frequent method to treat free moving boundary problems. For the details of the phase-field formulation and their numerical implementation we would like to refer the reader to the original

⁶ We should not confuse the mode $\ell = 1$ with the usual global translation, which is a neutral mode. Here only the external gel surface moves while the bead is fixed, so that the mode $\ell = 1$ is a physical one.

paper [28]. Here we shall only report the basic results

The numerical study in two dimensions with plane strain shows that for axisymmetric initial conditions with small amplitude perturbations, the symmetry is broken for the mode $m = 1$ (identical to the mode $\ell = 1$ in three dimensions), which corresponds to a translation of the gel layer with respect to the bead. Where this symmetry-breaking occurs, depends only on the initial conditions. The instability then evolves further into an actin comet, reminiscent of the comet developed by *Listeria monocytogenes*. Fig. 9 shows a typical result of a numerical simulation. The comet formation seems here to

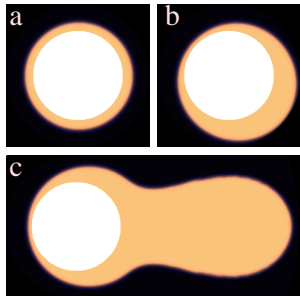


FIG. 9: Symmetry-breaking of a circular gel. Shown is the evolution of the gel thickness, starting from a homogeneous thin gel (a) with random small amplitude perturbations. (b) shows the initial symmetry breaking, while (c) shows the subsequent evolution of the shape into a comet in the far nonlinear regime (adapted from Ref. [28]).

be the generic growth mode. This finding points to the fact that the comet formation is probably a quite robust feature; it results from simple physical prototypes.

The physical picture of the symmetry breaking may be understood as follows. Let us start with a symmetric layer as in Fig. 9 (a). Suppose that due to some natural (inevitable) fluctuation, the gel layer becomes asymmetric, as in Fig. 9 (b). The stress is due to addition of new monomers at the bead/gel interface. On the side where the gel thickness is small the stress field is stronger than on the other side, since the gel feels more the “outwards pushing” of new monomers inserted at the bead. Because of the increase of the stress (and strain) in the thinner layer, polymerization becomes unfavorable there. New monomers will preferentially be inserted on the side where the thickness is larger. The appearance of modes larger than $\ell = 1$ would create several thin and thick regions, which are likely unfavorable. It seems thus that the mode $\ell = 1$ is optimal for the insertion of monomers at the bead/gel interface.

By considering also the stress dependent depolymerization at the external gel interface, one finds another instability, whereby the location of the most unstable mode is determined by surface tension. This result is in agreement with the occasional experimental observation of higher order modes [14], which will be discussed next within a more elaborate homogenization model.

4. Homogenization models

So far, continuous models have been suffering from the inadequate or insufficient description of the mechanical aspect of the actin gel. The greatest difficulty in the description of the mechanical equilibrium of the growing actin network arises from the fact, that the growth history determines the network structure and therefore also the stress distribution. Consequently, a realistic model would have to include the information on how the network evolved.

A second problem, which is most prominent in the description of the symmetry-breaking around solid objects, is the coupling of the growth process between the internal and the external interface. As an example, consider the problem of actin growth around a bead functionalized with ActA or Wasp/Scar: Typically growth takes place at the barbed end of the actin filaments, which points toward the bead/gel interface. This growth process pushes older gel layers further away from that interface. Experimentally, the growth process is observed by an increase in the gel thickness. However, it is not clear how the insertion of mass at a (fixed) solid/gel interface translates into the displacement of the (free) gel/liquid interface. A realistic elastic theory would have to account for this coupling problem in a rigorous way.

One observation, which might help to solve the above mentioned problems at least partly, is that the actin network forms more or less regular structures, which are not perfectly periodic, but could be considered in a first approximation as “almost periodic”. The actin gel can then be regarded abstractly as a network of elastic filaments connected by nodes with a certain periodicity. This network is completely defined by the positions of the nodes and their connectivities. In the network structure, the size of each elementary cell, e.g. the distance between two Arp2/3 crosslinks (\sim several tens nm), is small compared to the total size of the structure ($\sim 1 \mu\text{m}$), which introduces a small parameter η into the problem, which is the ratio of the length of the unit cell and the total network size. In the following we will shortly outline the basic idea of an actin homogenization model in two dimensions [10].

We consider a planar network of stiff elastic bars around a solid cylinder (radius r_0) with the topology shown in Fig. 10. The bars are connected to each other via nodes. The actin filaments are assumed to be linked to the cylinder at N_t sites evenly located on its surface at a distance $p = \eta r_0$ between two close sites, i.e. at an angular distance $\eta = \frac{2\pi}{N_t}$. The actin gel is made of N_n layers of bars in the radial direction. As the growth of the gel is due to the polymerization of actin monomers at the surface of the cylinder, each layer is assumed to be made up of the same number of nodes. So the nodes of the gel can be numbered by two integers (ν^1, ν^2) with ν^1 numbering the radial layers and ν^2 the position of the node in each layer, respectively.

It is assumed that the discrete net is made up of a large number of bars meaning that N_t and N_n are very large and of the same order. To be more precise, the parameter η is assumed to be very small and the number N_n of layers is given by $N_n = \frac{\alpha}{\eta}$ with α being of order 1 with respect to η . Using

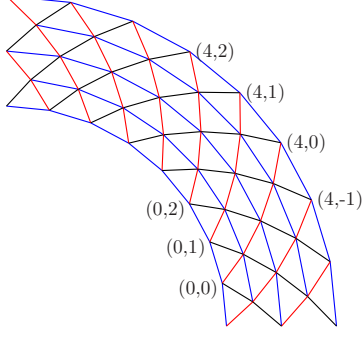


FIG. 10: Sketch of a small part of the filament network with some examples for the node numbering (ν^1, ν^2) . The “curves” along which $\nu^1 = \text{const.}$ and $\nu^2 = \text{const.}$ are shown in blue and red, respectively.

this notation, a node of the gel can be labeled by $(\mu^{1\eta}, \mu^{2\eta})$ with $\mu^{i\eta} = \eta\nu^i$. The coordinates $(\mu^{1\eta}, \mu^{2\eta})$ take values in $\omega =]0, \alpha[\times]0, 2\pi[$ and are meant to become the set of Lagrangian curvilinear coordinates of the equivalent continuous medium.

The upscaling of the net to a continuous medium consists in determining the equivalent stresses from the bar tensions, the equations of equilibrium (or motion) satisfied by these stresses and an equivalent constitutive equation ensuing from the properties of the bars. This can be carried out by using an asymptotic expansion (for an introduction see [9, 34, 54]). Here, as the network structure is simple, a more heuristic presentation can be used. The basic idea of the homogenization process is that, for most of the motions of the network, the positions of its nodes (ν^1, ν^2) can be approximated by a continuous function $\vec{\psi}(\nu^1, \nu^2)$ where $\mu^{i\eta} = \eta\nu^i$. The purpose then is to determine the equations governing this deformation function. The equivalent Cauchy stress tensor is given by the classical relation due to Cauchy [9, 34]

$$\sigma = \frac{1}{g} \sum_{b=1}^3 N^b \vec{e}^b \otimes \vec{B}^b \quad (30)$$

with \vec{B}^b being the “bar vector” linking the two extremities of the bar b ($b = 1, 2, 3$) of the elementary cell (shown in Fig. 11) (ν^1, ν^2) of the network in a deformed state, $\vec{e}^b = \frac{\vec{B}^b}{\|\vec{B}^b\|}$ being the corresponding unit vector, N^b the tension in the bar and $g = \|\vec{B}^1 \wedge \vec{B}^3\|$ being the surface of the elementary cell. The constitutive equation of the equivalent continuous medium follows from the constitutive equations of the bars which, for the sake of simplicity, are assumed to be

$$N^b = k^b \frac{l^b - l_m^b}{l_m^b} \quad (31)$$

with $l^b = \|\vec{B}^b\|$. l_m^b is the length of the bar b at rest and serves as a parameter in the constitutive equation.

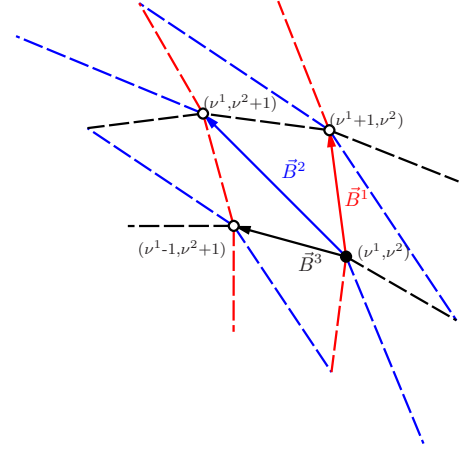


FIG. 11: Sketch of an elementary cell, showing the node numbering (ν^1, ν^2) and the elementary bar vectors \vec{B}^b (solid arrows). All other bars are shown as dashed lines. The “curves” along which $\nu^1 = \text{const.}$ and $\nu^2 = \text{const.}$ are shown in blue and red, respectively.

In order for a symmetrical equilibrium configuration of the gel to be possible, the constitutive equations of the bars 1 and 3 should be identical, i.e. $k^1 = k^3$ and $l_m^1 = l_m^3$.

Following the homogenization assumption stating that the position of the node (ν^1, ν^2) is $\vec{\psi}(\nu^1, \nu^2)$ with $\mu^{i\eta} = \eta\nu^i$, a simple Taylor expansion yields:

$$\begin{aligned} \vec{B}^1 &= \eta \left(\partial_1^\mu \vec{\psi} + \partial_2^\mu \vec{\psi} \right) \\ \vec{B}^2 &= \eta \partial_2^\mu \vec{\psi} \\ \vec{B}^3 &= \eta \left(-\partial_1^\mu \vec{\psi} + \partial_2^\mu \vec{\psi} \right) \end{aligned} \quad (32)$$

where $\partial_i^\mu = \frac{\partial}{\partial \mu^i}$. Since they are associated with a quite simple numbering system for the nodes, the variables μ^1 and μ^2 arise naturally as Lagrangian variables of the equivalent continuous medium through the homogenization process. However, they are not the most convenient variables to study symmetrical equilibrium configurations. Therefore we have introduced the variables λ^1 and λ^2 defined by

$$\lambda^1 = \mu^1 \text{ and } \lambda^2 = \frac{\mu^1}{2} + \mu^2. \quad (33)$$

Setting

$$\vec{\varphi}(\lambda^1, \lambda^2) = \vec{\psi} \left(\lambda^1, -\frac{\lambda^1}{2} + \lambda^2 \right) \quad (34)$$

one finds

$$\vec{B}^1 = \eta \vec{g}_1, \quad \vec{B}^2 = \eta \vec{g}_2 \text{ and } \vec{B}^3 = \eta \left(-\vec{g}_1 + \frac{1}{2} \vec{g}_2 \right) \quad (35)$$

with $\vec{g}_1 = \partial_1^\lambda \vec{\varphi}$ and $\vec{g}_2 = \partial_2^\lambda \vec{\varphi}$.

Carrying these relations into (30) yields

$$\sigma = \frac{1}{\|\vec{g}_1 \wedge \vec{g}_2\|} \sum_{i=1}^3 \vec{S}^i \otimes \vec{g}_i \quad (36)$$

with $\vec{S}^1 = \eta(N^1\vec{e}^1 - N^2\vec{e}^2)$ and $\vec{S}^2 = \eta(\frac{1}{2}N^1\vec{e}^1 + N^2\vec{e}^2 + \frac{1}{2}N^3\vec{e}^3)$.

As the only forces acting on the gel are applied on its boundaries, the equilibrium of the continuous medium reads classically

$$\text{div } \sigma = 0. \quad (37)$$

Using the virtual power formulation of that equation and the change of variables

$$(\lambda^1, \lambda^2) \leftrightarrow \vec{x} = \vec{\varphi}(\lambda^1, \lambda^2),$$

it can be proven that the equilibrium equation reads

$$\sum_{i=1}^2 \partial_i^\lambda \vec{S}^i = 0. \quad (38)$$

a. Coupling between growth and mechanics To study the growth of such an homogenized network, one can stay within the picture of a mechanical equilibrium of the actin gel on the time scale of the growth process. From the homogenized elastic equations one can derive the elastic contribution $\Delta\mu_e$ to the chemical potential $\Delta\mu$ for the addition or subtraction of nodes at the gel interfaces starting from the free elastic energy F_e in the network, i.e.

$$F_e = \frac{1}{\eta^2} \int_{\Omega} d\lambda^1 d\lambda^2 \sum_{b=1,2,3} f^b, \quad (39)$$

where f^b is the elastic energy associated with the extension or contraction of each of the filaments. The elastic chemical potential is then given by the variation of the elastic energy with respect to the size and shape of the network $\Delta\mu_e = \delta F_e / \delta \Omega$ by respecting the boundary conditions.

We assume now that the chemical potential contains also a contribution from the chemical process of polymerization $\Delta\mu_c$, where $\Delta\mu_c < 0$ at the internal interface and $\Delta\mu_c > 0$ at the external interface. This assumption accounts for the polar treadmilling behavior of the actin polymerization, i.e. polymerization occurs at the internal interface and depolymerization at the external interface. Furthermore, the chemical potential contains a contribution from interfacial energy, i.e. $\Delta\mu_s = -\gamma\kappa$, with γ being the surface tension coefficient and κ being the curvature of the interface. This leads to the following expression for the normal velocities of the two free interfaces in the Lagrangian coordinates (λ^1, λ^2)

$$v_n = -\eta M^i (\Delta\mu_e^i + \Delta\mu_c^i + \Delta\mu_s^i) = -\eta M^i \Delta\mu^i, \quad (40)$$

with $i = 0$ for the internal and $i = 1$ for the external interface.

b. Homogeneous gel growth and linear stability analysis First one may consider the symmetric problem, i.e. the growth of a gel with homogeneous thickness $\alpha = \eta N_n$ which has an axisymmetric solution $\vec{\varphi} = \varphi_r(\lambda_1)\vec{e}_r(\lambda_2)$. The equilibrium equation in this case then reduces to

$$0 = 2\partial_1^\lambda \left(\tilde{N}^1 \partial_1^\lambda \varphi_r \right) - \left(\frac{1}{2} \tilde{N}^1 + \tilde{N}^2 \right) \varphi_r, \quad (41)$$

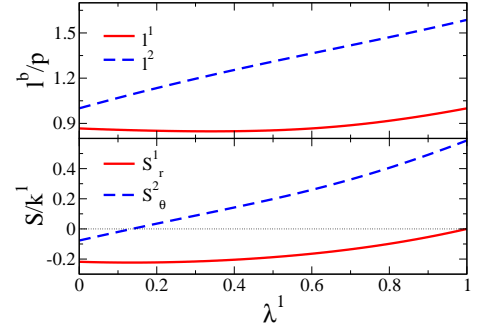


FIG. 12: Filament lengths (top), radial and tangential tensions (bottom) depending on the positions in the network in mechanical equilibrium. Parameters are $k^2/k^1 = 1$ and $l_m^1 = l_m^2 = p$.

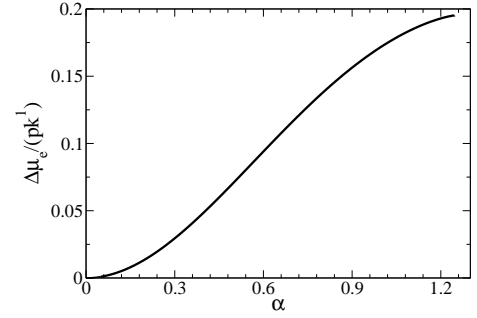


FIG. 13: Dependence of the elastic part of the chemical potential $\Delta\mu_e$ on the number of radial filament layers α . Remaining parameters are $l_m^1 = l_m^2 = p$ and $k^2/k^1 = 1$.

where we have introduced

$$\tilde{N}^b = \eta \frac{N^b}{l^b}. \quad (42)$$

In this situation the filaments with $b = 2$ are oriented in a tangential direction. Eq. (41) can be solved numerically using continuation methods [15].

Fig. 12 shows a solution of Eq. (41) for a given network thickness α . Naturally, l^2 is extending as one moves away from the bead, whereas l^1 is first shortening and then extending to reach its equilibrium length at the outer gel surface. Consequently, the gel is under radial compression and under tangential extension far away from the bead surface. However, for regions close to the bead surface the gel is under tangential compression.

Fig. 13 shows the dependence of the chemical potential depending on the number of radial filament layers α . Assuming that new filaments are inserted in the same stressed state as the already present material at the two interfaces, the elastic chemical potential is identical at the two interfaces for a homogeneous gel ($\Delta\mu_e^0 = \Delta\mu_e^1 = \Delta\mu_e$). With increasing network size, i.e. increasing α , $\Delta\mu_e$ increases in a strongly nonlinear fashion. Note, that for higher values of α the homogenization approach breaks down and the gel is starting to “fold back”. Beyond this point, at $\alpha \approx 1.25$ in Fig. 13, no

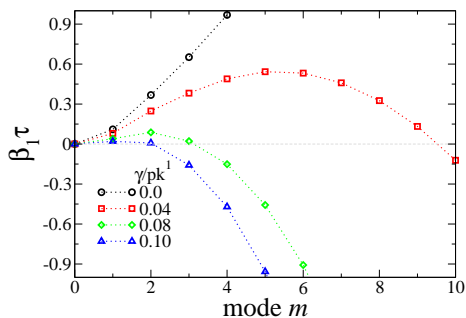


FIG. 14: Dispersion relation with Dirichlet boundary conditions at the internal interface. Shown is only the larger of two eigenvalues β_1 (the second one being always negative) depending on the wavenumber m for various values of the surface tension as indicated in the legend. Parameters are $\alpha = 1$, $k^2/k^1 = 1$, $l_m^1 = l_m^2 = p$. The time scale is $\tau = r_0/(Mk^1p^2)$.

physical meaningful solutions exist.

We consider now a filament network which is allowed to grow symmetrically with identical mobilities ($M^0 = M^1 = M$) at the two interfaces following the two dynamic equations

$$\partial_t \alpha^0 = \eta M (\Delta \mu_c^0 + \Delta \mu_e) = -v_p + v_e \quad (43)$$

$$\partial_t \alpha^1 = -\eta M (\Delta \mu_c^1 + \Delta \mu_e) = -v_d - v_e \quad (44)$$

whereby the positions of the internal and external interface are denoted by α^0 and α^1 , and where we have introduced the polymerization speed $v_p = -\eta M \Delta \mu_c^0 > 0$, the depolymerization speed $v_d = \eta M \Delta \mu_c^1$ and an “elastic speed” $v_e = \eta M \Delta \mu_e$. The steady state for the gel thickness is given by $\partial_t \alpha = \partial_t \alpha^1 - \partial_t \alpha^0 = 0$. Defining now a mean velocity $\bar{v} = (v_p + v_d)/2$ and a velocity difference $\Delta v = (v_p - v_d)/2$, one obtains that in the steady state $\Delta v = v_e$ and $\partial_t \alpha^0 = \partial_t \alpha^1 = -\bar{v}$. This means that, although the gel thickness does not change, both interfaces are moving with the same velocity $-\bar{v}$ and therefore, \bar{v} has the physical meaning of the tread-milling speed.

If we now transform the dynamical equations into the co-moving frame moving with velocity $-\bar{v}$ in the direction of λ^1 we can study the linear stability of the network thickness α with respect to perturbations of the type $\cos(m\lambda^2)$ at the internal and external interface, $\epsilon^0(\lambda^2)$ and $\epsilon^1(\lambda^2)$, respectively,

Fig. 14 shows the dispersion relation for the largest growth rate depending on the wavenumber m . One of two eigenvalues is always negative (i.e. stable), whereas the other one can be positive (unstable) depending on surface tension. We did not find a threshold value for the filament layer number, beyond which the gel becomes stable towards small perturbations independent of the surface tension. However, a higher surface tension can suppress instabilities for thin gels. Recent experiments have shown the occurrence of higher modes than one, i.e. the formation of up to three actin comets around one bead [14], depending on the experimental conditions. The actual value for the surface tension of an actin network against water should be rather small, since actin is a soluble protein. Furthermore, typically small beads with higher

curvature break the symmetry faster, than larger beads [58], which is in agreement with our model, where the time scale of symmetry-breaking increases linearly with the radius of the bead r_0 . Note also that, assuming a constant polymerization potential, but changing the radius r_0 by keeping all other parameters constant, leads to a linear relation between the gel thickness, i.e. $\varphi_r(\alpha) - \varphi_r(0)$, and r_0 in steady state. These two results have also been obtained in simpler models based on scaling arguments [41, 48, 58] and hold for the case that monomer diffusion is fast enough to avoid depletion of monomers due to polymerization at the internal bead gel interface. Another interesting point is the type of instability one might observe, i.e. an undulating vs. peristaltic instability. For small modes $m \leq 4$ one finds an undulating instability, i.e. the perturbations at the external and internal interface are in phase, whereas for higher order modes one should observe a peristaltic instability, where the two perturbations have the opposite phase (data not shown).

IV. CONCLUSIONS AND PERSPECTIVES

In this chapter we have tried to summarize the complex properties and out-of-equilibrium phenomena of actin gels linked by the Arp2/3 complex, which are at the origin of the motility of animal cells, as well as of intracellular organelles and pathogens. Primarily, we have focused on two subjects: the complex actin polymerization dynamics under load at the polymer brush, and the symmetry-breaking of actin gels grown from the surface of small objects. While we have treated both subjects separately, it is obvious that a full understanding of the system will have to include both approaches: the macroscopic stress distribution in the actin gel couples to the polymerization kinetics in the polymer brush, which in turn changes the deformation state of the gel and the macroscopic stress distribution. We have shown in the previous paragraphs that homogenization models are at the moment the most appropriate models to capture the complex microscopic structures of biological materials on the one hand and take advantage of a continuous framework on the other hand. We believe, that the future in the modeling of growing actin gels in complex geometries, e.g. the advancing cell edge, lies in the coupling of these homogenization models to a complex dynamics in the polymer brush, as proposed e.g. in Refs. [16, 21].

An important question that remains to be elucidated is, how motion can be generated once the gel layer has become asymmetric. So far we have either limited our considerations to the case of a symmetry-breaking around objects, and neglected the generation of motion, or, as in most microscopic models, we have only considered a stationary actin comet, which pushes an obstacle by polymerization. Both concepts are circumventing, by more or less hand waving arguments, one critical question. What is the origin of motion in the absence of external forces, provided that the actin comet and the object are only surrounded by a newtonian viscous fluid (recall that we are in a regime with $Re \ll 1$) and not attached to some support. Recently, Prost et al. [48] has put forward a simple

argument based on largely disparate friction coefficients for the obstacle and the actin tail and the property of treadmilling. In the following we will outline this argument.

Suppose that an obstacle and its associated actin comet move with velocities \mathbf{v}_o and \mathbf{v}_c , respectively, in the laboratory frame. In the viscous regime the force balance reads then

$$0 = \xi_o \mathbf{v}_o + \xi_c \mathbf{v}_c, \quad (45)$$

where ξ_o and ξ_c denote the friction coefficients of the object and the comet with the surrounding fluid, respectively. The difference in the two velocities $\mathbf{v}_t = \mathbf{v}_o - \mathbf{v}_c$ is the treadmilling speed. Substituting \mathbf{v}_c in Eq. (45) and after some rearrangement one finds for the object velocity

$$\mathbf{v}_o = \mathbf{v}_t \frac{\xi_c}{\xi_o + \xi_c}. \quad (46)$$

This means, that although the dissipation due to fluid friction is very small, it plays nevertheless a decisive role, since it is the ratio of friction coefficients which determines the object velocity. In the limit of $\xi_c \gg \xi_o$ this velocity approaches the treadmilling speed. Given the fact, that the actin comet is much larger than the object, e.g. bead, droplet or vesicle,

which causes a much larger friction, the experimentally observed obstacle velocities are indeed close to the treadmilling speed.

Another biological aspect, which might be of importance when considering more complex cellular systems is the fact that the actin polymerization system is not constitutively active as in *in vitro* assays but is regulated by signaling cascades, which constitute in itself a nonlinear dynamical system. Typically these signaling cascades are modeled by reaction-diffusion systems which lead to pattern formation [37], e.g. polarization of the cell into leading and advancing edge. It remains to be shown how these two important mechanisms, elastic instabilities and instabilities due to reaction-diffusion processes, integrate to produce cellular motion.

Acknowledgements: C.M. and K.J. acknowledge financial support from the CNES and the Alexander von Humboldt Foundation, and with D.C., M.I., P.P., and A.R. we acknowledge a financial support from ANR MOSICOB (MODélisation et SIMulation de fluides COMplexes Biomimétiques).

-
- [1] M. Abercrombie (1980) The crawling movement of metazoan cells. *Proc. R. Soc. London B* **207**:129–147, and references therein.
- [2] J.B. Alberts and G.M. Odell (2004) In silico reconstitution of *Listeria* propulsion exhibits nano-saltation. *PLoS Biol.* **2**:e412.
- [3] K.I. Anderson and R. Cross (2000) Contact dynamics during keratocyte motility. *Curr. Biol.* **10**:253–260.
- [4] A. Bernheim-Groswasser, J. Prost and C. Sykes (2005) Mechanism of actin-based motility: A dynamic state diagram. *Bioophys. J.* **89**:1411–1419.
- [5] A. Bernheim-Groswasser, S. Wiesner, R.M. Golsteyn, M.-F. Carlier and C. Sykes (2002) The dynamics of actin-based motility depend on surface parameters. *Nature* **417**:308–311.
- [6] H. Boukellal, O. Campás, J.-F. Joanny, J. Prost and C. Sykes (2004) Soft *Listeria*: Actin-based propulsion of liquid drops. *Phys. Rev. E* **69**:061906.
- [7] D. Bray (1992) *Cell movements*, New York & London, Garland Publishing, Inc..
- [8] N.J. Burroughs and D. Marenduzzo (2007) Nonequilibrium-driven motion in actin networks: Comet tails and moving beads. *Phys. Rev. Lett.* **98**:238302.
- [9] D. Caillerie and B. Cambou (2001) Les techniques de changement d'échelles dans les matériaux granulaires, in *Micromécanique des milieux granulaires*, Paris, Hermès Sciences.
- [10] D. Caillerie, K. John, N. Meunier, C. Misbah, P. Peyla and A. Raoult (2009) A model for actin driven motility through discrete homogenization. *manuscript in preparation*.
- [11] L.A. Cameron, M.J. Footer, A. Van Oudenaarden and J.A. Theriot (1999) Motility of ActA protein-coated microspheres driven by actin polymerization. *Proc. Natl Acad. Sci. USA* **96**:4908–4913.
- [12] A.E. Carlsson (2001) Growth of branched actin networks against obstacles. *Biophys. J.* **81**:1907–1923.
- [13] S. Cudmore, P. Cossart, G. Griffiths and M. Way (1995) Actin-based motility of *Vaccinia* virus. *Nature* **378**:636–638.
- [14] V. Delatour, S. Shekhar, A.-C. Reyman, D. Didry, K. Hô Diêp Lê, G. Romet-Lemonne, E. Helfer and M.-F. Carlier (2008) Actin-based propulsion of functionalized hard versus fluid spherical objects. *New J. Phys.* **10**:025001.
- [15] E.J. Doedel, A.R. Champneys, T.F. Fairgrieve, Y.A. Kuznetsov, B. Sandstede and X.J. Wang (1997) *AUTO97: Continuation and bifurcation software for ordinary differential equations*, Montreal, Concordia University.
- [16] M. Enculescu, A. Gholami and M. Falcke (2008) Dynamic regimes and bifurcations in a model of actin-based motility. *Phys. Rev. E* **78**:031915.
- [17] D.A. Fletcher and J.A. Theriot (2004) An introduction to cell motility for the physical scientist. *Phys. Biol.* **1**:T1–T10.
- [18] Y. Fukui and S. Inoué (1997) Amoeboid movement anchored by eupodia, new actin-rich knobby feet in *Dictyostelium*. *Cell Motil. Cytoskel.* **36**:339–354.
- [19] F. Gerbal, P. Chaikin, Y. Rabin and J. Prost (2000) An elastic analysis of *Listeria monocytogenes* propulsion. *Biophys. J.* **79**:2259–2275.
- [20] F. Gerbal, V. Laurent, A. Ott, M.-F. Carlier, P. Chaikin and J. Prost (2000) Measurement of the elasticity of the actin tail of *Listeria monocytogenes*. *Eur. Biophys. J.* **29**:134–140.
- [21] A. Gholami, M. Falcke and E. Frey (2008) Velocity oscillations in actin-based motility. *New J. Phys.* **10**:033022.
- [22] A. Gholami, J. Wilhelm and E. Frey (2006) Entropic forces generated by grafted semiflexible polymers. *Phys. Rev. E* **74**:041803.
- [23] P.A. Giardini, D.A. Fletcher and J.A. Theriot (2003) Compression forces generated by actin comet tails on lipid vesicles. *Proc. Natl Acad. Sci. USA* **100**:6493–6498.
- [24] M.B. Goldberg and J.A. Theriot (1995) *Shigella flexneri* surface protein IcsA is sufficient to direct actin-based motility. *Proc. Natl Acad. Sci. USA* **92**:6572–6576.

- [25] K.C. Holmes, D. Popp, W. Gebhard and W. Kabsch (1990) Atomic model of the actin filament. *Nature* **347**:44–49.
- [26] J. Howard (2001) *Mechanics of motor proteins and the cytoskeleton*, Sinauer Associates, Inc.
- [27] G. Isenberg, P.C. Rathke, N. Hülsmann, W.W. Franke and K.E. Wohlfahrt-Bottermann (1976) Cytoplasmic actomyosin fibrils in tissue culture cells. Direct proof of contractility by visualization of ATP-induced contraction in fibrils isolated by laser microbeam dissection. *Cell Tiss. Res.* **166**:427–443.
- [28] K. John, P. Peyla, K. Kassner, J. Prost and C. Misbah (2008) A nonlinear study of symmetry-breaking in actin gels - Implications for cellular motility. *Phys. Rev. Lett.* **100**:068101.
- [29] M. Kaksonen, C.P. Toret and D.G. Drubin (2006) Harnessing actin dynamics for clathrin-mediated endocytosis. *Nat. Rev. Mol. Cell. Biol.* **7**:404–414.
- [30] M. Krupa and P. Szmolyan (2001) Relaxation oscillation and canard explosion. *J. Differ. Equations* **174**:312 – 368.
- [31] I. Lasa, E. Gouin, M. Goethals, K. Vancompennolle, V. David, J. Vandekerckhove and P. Cossart (1997) Identification of two regions in the N-terminal domain of ActA involved in the actin comet tail formation by *Listeria monocytogenes*. *EMBO J.* **16**:1531–1540.
- [32] A. Lee, H.Y. Lee and M. Kardar (2005) Symmetry-breaking motility. *Phys. Rev. Lett.* **95**:138101.
- [33] T.P. Loisel, R. Boujemaa, D. Pantaloni and M.-F. Carlier (1999) Reconstitution of actin-based motility of *Listeria* and *Shigella* using pure proteins. *Nature* **401**:613–616.
- [34] A.E.H. Love (1944) *A treatise of the mathematical theory of elasticity*, New York, Dover Publications.
- [35] L. Ma, L.C. Cantley, P.A. Janmey and M.W. Kirschner (1998) Corequirement of specific phosphoinositides and small GTP-binding protein Cdc42 in inducing actin assembly in *Xenopus* egg extracts. *J. Cell Biol.* **140**:1125–1136.
- [36] Y. Marcy, J. Prost, M.-F. Carlier and C. Sykes (2004) Forces generated during actin-based propulsion: A direct measurement by micromanipulation. *Proc. Natl Acad. Sci. USA* **101**:5992–5997.
- [37] A.F.M. Marée, A. Jilkiné, A. Dawes, V.A. Grieneisen and L. Edelstein-Keshet (2006) Polarization and movement of keratocytes: A multiscale modelling approach. *Bull. Math. Biol.* **68**:1169–1211.
- [38] A. Michelot, J. Berro, C. Guérin, R. Boujemaa-Paterski, C. J. Staiger, J.-L. Martiel and L. Blanchoin (2007) Actin-filament stochastic dynamics mediated by ADF/Cofilin. *Curr. Biol.* **17**:825–833.
- [39] A. Mogilner and G. Oster (1996) Cell motility driven by actin polymerization. *Biophys. J.* **71**:3030–3045.
- [40] A. Mogilner and G. Oster (2003) Force generation by actin polymerization II: The elastic ratchet and tethered filaments. *Biophys. J.* **84**:1591–1605.
- [41] V. Noireaux, R.M. Golsteyn, E. Friederich, J. Prost, C. Antony, D. Louvard and C. Sykes (2000) Growing an actin gel on spherical surfaces. *Biophys. J.* **78**:1643–1654.
- [42] A. Ott, M. Magnasco, A. Simon and A. Libchaber (1993) Measurement of the persistence length of polymerized actin using fluorescence microscopy. *Phys. Rev. E* **48**:R1642–R1645.
- [43] S.H. Parekh, O. Chaudhuri, J. A. Theriot and D. A. Fletcher (2005) Loading history determines the velocity of actin-network growth. *Nature Cell Biol.* **7**:1219–1223.
- [44] C.S. Peskin, G.M. Odell and G.F. Oster (1993) Cellular motions and thermal fluctuations: The brownian ratchet. *Biophys. J.* **65**:316–324.
- [45] J. Plastino, I. Lelidis, J. Prost and C. Sykes (2004) The effect of diffusion, depolymerization and nucleation promoting factors on actin gel growth. *Eur. Biophys. J.* **33**:310–320.
- [46] T.D. Pollard, L. Blanchoin and R.D. Mullins (2000) Molecular mechanisms controlling actin filament dynamics in nonmuscle cells. *Ann. Rev. Biophys. Biomol. Struct.* **29**:545–576.
- [47] T.D. Pollard and G.G. Borisy (2003) Cellular motility driven by assembly and disassembly of actin filaments. *Cell* **112**:453–465.
- [48] J. Prost, J.-F. Joanny, P. Lenz and C. Sykes (2008) The physics of *Listeria* propulsion, in *Cell Motility*, 1–30, New York, Springer.
- [49] S.M. Rafelski and J.A. Theriot (2004) Crawling toward a unified model of cell motility: Spatial and temporal regulation of actin dynamics. *Annu. Rev. Biochem.* **73**:209–239.
- [50] K. Sekimoto, J. Prost, F. Jülicher, H. Boukellal and A. Bernheim-Grosswasser (2004) Role of tensile stress in actin gels and a symmetry-breaking instability. *Eur. Phys. J. E* **13**:247–259.
- [51] L. Stryer (1995) *Biochemistry*, New York, W. H. Freeman & Company.
- [52] J.A. Theriot and T.J. Mitchison (1991) Actin microfilament dynamics in locomoting cells. *Nature* **352**:126–131.
- [53] T.A. Theriot, T.J. Mitchison, L.G. Tilney and D.A. Portnoy (1992) The rate of actin-based motility of intracellular *Listeria monocytogenes* equals the rate of actin polymerization. *Nature* **357**:257–260.
- [54] H. Tollenaere and D. Caillerie (1998) Continuous modeling of lattice structures by homogenization. *Adv. Eng. Software* **29**:699–705.
- [55] L. Trichet, O. Campàs, C. Sykes and J. Plastino (2007) VASP governs actin dynamics by modulating filament anchoring. *Biophys. J.* **92**:1081–1089.
- [56] A. Upadhyaya, J.R. Chabot, A. Andreeva, A. Samadani and A. van Oudenaarden (2003) Probing polymerization forces by using actin-propelled lipid vesicles. *Proc. Nat. Acad. Sci. USA* **100**:4521–4526.
- [57] M. Urbakh, J. Klafter, D. Gourdon and J. Israelachvili (2004) The nonlinear nature of friction. *Nature* **430**:525–528.
- [58] J. van der Gucht, E. Paluch, J. Plastino and C. Sykes (2005) Stress release drives symmetry breaking for actin-based movement. *Proc. Natl Acad. Sci. USA* **102**:7847–7852.
- [59] A. van Oudenaarden and J.A. Theriot (1999) Cooperative symmetry-breaking by actin polymerization in a model for cell motility. *Nature Cell Biol.* **1**:493–499.
- [60] A.B. Verkhovskiy, T.M. Svitkina and G.G. Borisy (1999) Self-polarization and directional motility of cytoplasm. *Curr. Biol.* **9**:11–20.
- [61] S. Wiesner, E. Helfer, D. Didry, G. Ducouret, F. Lafuma, M.-F. Carlier and D. Pantaloni (2003) A biomimetic motility assay provides insight into the mechanism of actin-based motility. *J. Cell Biol.* **160**:387–398.
- [62] D. Yazar, W. To, A. Abo and M.D. Welch (1999) The Wiskott-Aldrich syndrome protein directs actin-based motility by stimulating actin nucleation with the Arp2/3 complex. *Curr. Biol.* **9**:555–558.